Helium ions for radiotherapy? Physical and biological verifications of a novel treatment modality

Michael Krämer,[a] Emanuele Scifoni, Christoph Schuy, and Marta Rovituso
Biophysics, GSI Helmholtzzentrum für Schwerionenforschung GmbH, Planckstr. 1, 64291 Darmstadt, Germany

Walter Tinganelli
Biophysics, GSI Helmholtzzentrum für Schwerionenforschung GmbH, Planckstr. 1, 64291 Darmstadt, Germany and Trento Institute for Fundamental Physics and Application (TIFPA-INFN), 38123, via Sommarive 14, Trento, Italy

Andreas Maier, Robert Kaderka, and Wilma Kraft-Weyrather
Biophysics, GSI Helmholtzzentrum für Schwerionenforschung GmbH, Planckstr. 1, 64291 Darmstadt, Germany

Stephan Brons and Thomas Tessonnier
Heidelberger Ionenstrahl-Therapiezentrum (HIT), Im Neuenheimer Feld 450, 69120 Heidelberg, Germany and Radioonkologie und Strahlentherapie, Universitätsklinikums Heidelberg, Im Neuenheimer Feld 400, 69120 Heidelberg, Germany

Katia Parodi
Heidelberger Ionenstrahl-Therapiezentrum (HIT), Im Neuenheimer Feld 450, 69120 Heidelberg, Germany; Radioonkologie und Strahlentherapie, Universitätsklinikums Heidelberg, Im Neuenheimer Feld 400, 69120 Heidelberg, Germany; and Ludwig-Maximilians-Universitaet Muenchen (LMU Munich), Department of Medical Physics, Am Coulombwall 1, 85748 Munich, Germany

Marco Durante
Biophysics, GSI Helmholtzzentrum für Schwerionenforschung GmbH, Planckstr. 1, 64291 Darmstadt, Germany and Trento Institute for Fundamental Physics and Application (TIFPA-INFN), 38123, via Sommarive 14, Trento, Italy

(Received 24 August 2015; revised 3 March 2016; accepted for publication 8 March 2016; published 30 March 2016)

Purpose: Modern facilities for actively scanned ion beam radiotherapy allow in principle the use of helium beams, which could present specific advantages, especially for pediatric tumors. In order to assess the potential use of these beams for radiotherapy, i.e., to create realistic treatment plans, the authors set up a dedicated ^{4}He beam model, providing base data for their treatment planning system TRiP98, and they have reported that in this work together with its physical and biological validations.
Methods: A semiempirical beam model for the physical depth dose deposition and the production of nuclear fragments was developed and introduced in TRiP98. For the biological effect calculations the last version of the local effect model was used. The model predictions were experimentally verified at the HIT facility. The primary beam attenuation and the characteristics of secondary charged particles at various depth in water were investigated using ^{4}He ion beams of 200 MeV/u. The nuclear charge of secondary fragments was identified using a $\Delta E/E$ telescope. 3D absorbed dose distributions were measured with pin point ionization chambers and the biological dosimetry experiments were realized irradiating a Chinese hamster ovary cells stack arranged in an extended target.
Results: The few experimental data available on basic physical processes are reproduced by their beam model. The experimental verification of absorbed dose distributions in extended target volumes yields an overall agreement, with a slight underestimation of the lateral spread. Cell survival along a 4 cm extended target is reproduced with remarkable accuracy.
Conclusions: The authors presented a simple simulation model for therapeutical ^{4}He beams which they introduced in TRiP98, and which is validated experimentally by means of physical and biological dosimetries. Thus, it is now possible to perform detailed treatment planning studies with ^{4}He beams, either exclusively or in combination with other ion modalities. [http://dx.doi.org/10.1118/1.4944593]

Key words: ion beam radiotherapy, helium ions, treatment planning system

1. INTRODUCTION

Radiotherapy with heavy charged particles is an established option for the treatment of certain kinds of tumors. Most heavy charged particle treatments are nowadays performed with protons and carbon ions (Table I). There is, however, some room for unconventional beams other than these two ions. Whereas the usage of pions certainly is history, there is growing interest, for example, in fast helium ion beams. To some extent, they fill the gap between protons and carbon ions. From the physical point of view, they might be advantageous since they cause less projectile fragmentation than carbon ions and less lateral beam spread than protons (see Fig. 1). From the radiobiological point of view, their Relative Biological Effectiveness (RBE) is closer to protons, though not negligible, but certainly lower than that of carbon ions. This might be beneficial in certain treatment situations, for example, for pediatric patients.

Pioneering work was performed at LBNL (Berkeley, USA), with some 2000 patients treated with ^{4}He using a passive beam delivery.[1] With the advent of therapy facilities like HIT (Heidelberg, Germany),[2] CNAO (Pavia, Italy),[3] and soon MedAustron (Wiener Neustadt, Austria),[4] equipped with active beam delivery systems and providing multiple ion species from protons through oxygen, a revival of ^{4}He ions is not unrealistic. For this to happen, however, the relevant physical and radiobiological characteristics of ^{4}He ions interacting with biological matter need to be investigated in a similar fashion, as was done for carbon ions. To achieve this goal, a beam model for a Treatment Planning System (TPS) has to be created and verified, which is the intention of this paper.

It is outlined as follow: in material and methods we shortly introduce our treatment planning system, TRiP98, we describe the experimental equipment used for verification and report on the newly developed pragmatic beam model for therapeutic ^{4}He ions. In Sec. 3 we report dosimetric results for absorbed dose as well as cell survival distributions. We conclude with a short discussion.

2. MATERIALS AND METHODS

2.A. Treatment planning system

One of the first steps for extending the treatment of cancer patients to novel ion modalities is the development of a TPS. The natural choice is the well established TRiP98,[6–8] developed in-house for clinical use during the carbon ion pilot project at GSI.[9] It also served as a prototype for the commercial Siemens SynGo PT planning system, which is currently in use at various ion beam radiotherapy sites [HIT, CNAO, Shanghai, MIT (Marburg, Germany)]. Since the end of the pilot project, it is used for research purposes, available also outside GSI under certain conditions. Its flexible, largely table-driven design allows to import new base data sets such as depth dose distributions, particle spectra, and RBE tables. It is constantly developed and enhanced and thus is the ideal tool to investigate new beam modalities and their specific applications.[10,11]

TABLE I. Patient numbers by Dec-2013 (Ref. 5).

Ion	Past	Current	Site
Protons		105 743	
C-ions		13 119	
Pions	1100		LANL, PSI, TRIUMF
He-ions	2054		LBNL
Other ions	433		LBNL

2.B. Experimental setup

2.B.1. Irradiation system

All experiments were performed at the Quality Assurance (QA) room at HIT. The horizontal beam line is equipped with five monitor chambers (two for position and three for intensity control) on its outlet. The treatment plans were realized considering the HIT available pool of monoenergetic pencil beams, with specific energies, intensities, and beam spot sizes. For basic physics experiments, a beam of ^{4}He at 200 MeV/u was delivered by RF knockout extraction from the synchrotron. A monoenergetic pencil beam with a spot size of approximately 5 mm FWHM measured at the isocenter, i.e., 1.05 m from the beam nozzle. The beam intensity was 1000 particles/s, which is much below clinical levels, but necessary for typical single particle physics measurements. Higher beam intensities will cause pile-up of particle signals in the detector, will lead to excessive dead-time in the electronics

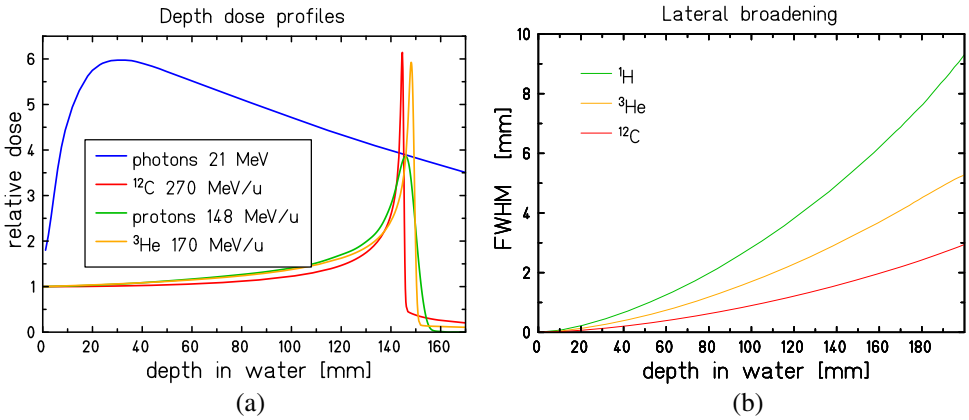

FIG. 1. (a) Depth dose distributions, (b) lateral beam spread for various beam modalities.

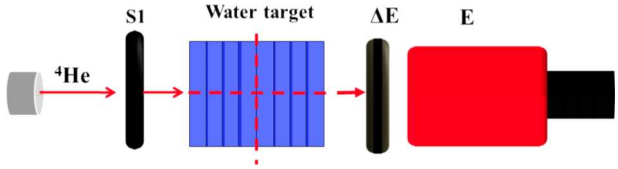

FIG. 2. Experimental setup to measure beam attenuation and fragment buildup.

and data acquisition system and ultimately might even damage the BaF_2 detector. For therapy conditions, the intensity is much higher, up to 8.0×10^8 particles/s.

2.B.2. Setup for basic physics data

For studying the absorption of primary ^{4}He ions as a function of water depth, the setup shown in Fig. 2 was used. Particles exiting the beam line were monitored and counted with a 1 mm thick plastic scintillator placed downstream of the exit window. The surviving ^{4}He ions together with the lighter fragments produced by nuclear fragmentation were identified by a telescope system consisting of a 9 mm thick plastic scintillator with hexagonal shape and a 14 cm long BaF_2 detector of hexagonal shape with an inscribed circle radius of 4.5 cm placed behind the water target. The target consisted of several polystyrene flasks (manufactured by COSTAR). The outer dimensions of each flask were $x = 11.9$ cm, $y = 20.0$ cm, and $z = 4.26$ cm, where x and y denote the lateral size and height (both perpendicular to the beam axis), and z the extension along the beam direction. The material traversed by the beam particles was 3.8 cm water and 0.42 cm polystyrene (entrance and exit wall) for each flask. The total water-equivalent thickness of one flask was 4.229 cm. We used 1, 2, 4, 5, and 6 flasks to measure the particle yield at water equivalent depths of 4.2, 8.4, 16.8, 21, and 25.2 cm, respectively. The water target central axis was aligned to the isocenter (See Fig. 2). Charged particles emerging from the water target were identified in a 2D scatter plot of energy loss versus residual energy ($\Delta E - E$, Fig. 3) using a graphical window.[12,13] The identification of particles with different charge number Z and mass number A is not unambiguous. We estimate the uncertainty of the measured yield to be 2% for the helium isotopes and 9% for the hydrogen isotopes.

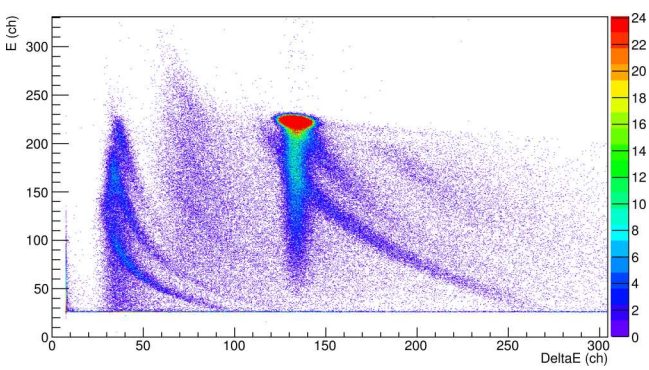

FIG. 3. Residual energy versus energy loss scatter plot for a 200 MeV/u ^{4}He beam on 17 cm of water.

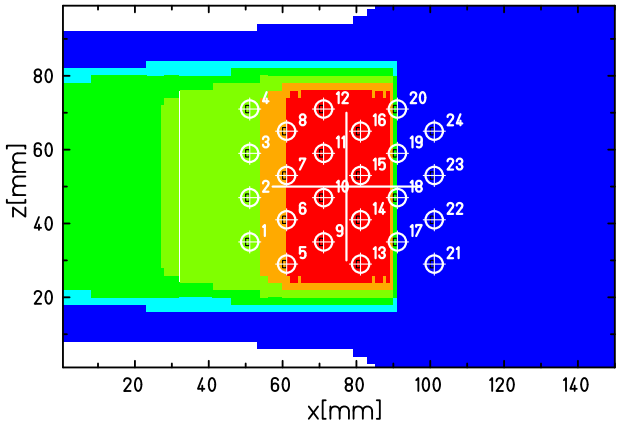

FIG. 4. Two-dimensional arrangement of pin point chambers to measure absorbed dose distributions. Actually it is a projection of the three dimensional configuration onto the (x, z) plane. The first and last two lines along z are staggered, respectively, ±6 mm in y direction.

2.B.3. 3D dosimetry

Absorbed dose distributions in irradiation plans were measured with a set of pin point chambers [Multidos, PTW (Refs. 14 and 15)] in a conventional water phantom. The arrangement comprises a set of 24 pin point ionization chambers with a sensitive volume of 0.03 cm^3 and a diameter of 2.9 mm, as shown in the xz plane projection of Fig. 4. The six rows along z are staggered on three different y levels (see Ref. 14 for details). It can be moved in x-, y-, and z-direction with a resolution of 0.1 mm, in order to collect more data points for a given cut through the dose distribution.

2.B.4. Biological dosimetry

Cell survival distributions as a function of depth were measured with the stack setup shown in Fig. 5.

The $5\times10\times16$ cm^3 PMMA holder, typically used in our group for extended target volume irradiations (see Ref. 16 for details), allows to place polystyrene slices holding cell monolayers in several slots, with a resolution of 5 mm along the beam direction. We selected our standard cell line, Chinese hamster ovary cells (CHO-K1). This particular cell line has the advantages of easy handling, regular growth under difficult conditions, good reproducibility of results, and an α/β ratio comparable to several human tissues. Moreover, in our group, CHO cells were used with many different ions, in particular, carbon and protons,[16] which facilitates comparisons with previous data. For modeling purposes, other cell lines such as V79 or Human Salivary Gland (HSG) are of course also conceivable, because the validity of our radiobiological model does not depend on a particular cell line. Fifty thousand CHO-K1 cells were seeded in each of these 25 cm^2 slices 24 h before irradiation, and after irradiation they were trypsinized, measuring cell survival according to the standard procedure.[17] In order to increase the resolution in depth, and to obtain a denser measurement grid especially in the region of the highest dose gradient, two different setups were used. In one of the two configurations (setup B), an additional layer of

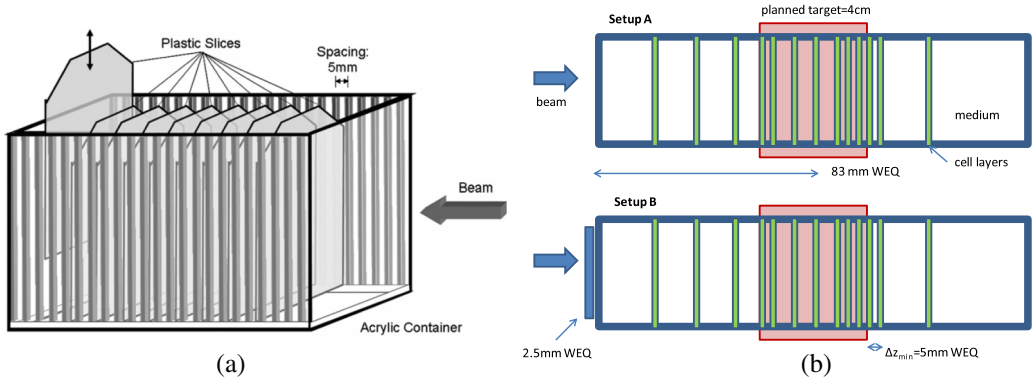

FIG. 5. Experimental device used for one dimensional cell survival distribution measurement. On the left, the overall sketch of the device comprising several slots for slices supporting cell layers; on the right, top view showing the specific sampling points (slots) which were chosen with respect to the planned target volume and the two different setups used for increasing the depth resolution. WEQ denotes "Water EQuivalent."

material (polystyrene) was added [see Fig. 5(b)], to shift all the sampling points by 2.51 mm. The slight modification in the water equivalent path length induced by each slice of polystyrene (factor 1.04) was accounted for. Clonogenic cell survival assay was performed. For each setup, the results were collected from two independent experiments, as average and standard deviation (error bars). Considering the variability of the cell's radiosensitivity (Subsection 3.C), we thought that, having only two measurements, the standard deviation would be more appropriate as a confidence interval. In each of the experiments the survival was determined by three technical replicates used for seeding, i.e., different replicated samples of colonies were seeded and counted from the same irradiated sample.

2.C. Physical beam model

Previous approaches used a pencil beam model of the absorbed dose distribution to describe therapeutic ^{4}He ion beams.[18] While this is the natural first step, it is not enough to enable realistic treatment planning including radiobiological effects, which is the state of-the-art for our TRiP98 TPS.

Establishing a physical beam model for our purposes requires a set of basic information: energy loss tables (dE/dx) for all participating primary and secondary ions, nuclear reaction cross sections describing the loss of primary beam particles, and fragmentation cross sections to calculate the build up of secondary ions as the beam traverses matter.

Electromagnetic energy losses are calculated according to Salamon.[19] Assuming an average ionization potential of 77 eV, the agreement between calculated and measured Bragg peak positions is within 0.5 mm for a variety of light ions at therapeutic energies. This choice of the ionization potential is indeed somewhat arbitrary. To the best of our knowledge no *ab initio* calculation with sufficient accuracy exists for this quantity. A sensitivity analysis reveals that the position of the Bragg peak shifts by ≈0.3 mm for 1 eV shift of the ionization potential. The pragmatic way to deal with this situation is to fine tune this value according to the measured Bragg peak position for a few selected beam energies. The description of nuclear interactions is more difficult, since only few experimental data are available for hydrogen and oxygen targets and classical reaction models like Silberberg and Tsao[20] are less suited for collision systems in the therapeutical range. A semiempirical model at least partially suited for our purposes was proposed by Cucinotta *et al.*[21] It assumes two-body dissociation of light ions to predict fragmentation cross sections. Since our main target is water (as a substitute for soft

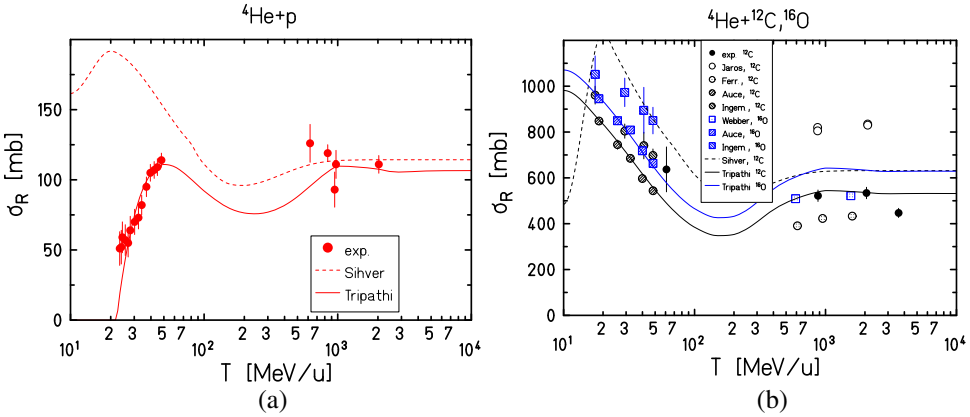

FIG. 6. Total reaction cross sections for ^{4}He on p, ^{12}C, and ^{16}O targets as a function of the energy. Symbols are experimental data taken from Refs. 25 and 26 (p), Refs. 27–31 (^{12}C), and Refs. 27, 30, and 31 (^{16}O).

TABLE II. Breakup channels of ^{4}He on p (Ref. 32).

Reaction	Threshold (MeV)
$^4He + p \rightarrow {}^2H + {}^3He$ (pickup)	22.94
$\rightarrow p + p + {}^3H$	24.77
$\rightarrow p + n + {}^3He$	25.72
$\rightarrow p + {}^2H + {}^2H$ (pickup)	29.81
$\rightarrow p + p + n + {}^2H$	32.59
$\rightarrow p + p + p + n + n$	35.37

tissue), we have to treat collisions of ^{4}He with protons as well as with oxygen nuclei.

2.C.1. Total reaction cross sections

Total reaction cross sections are conveniently described by variants of the Bradt–Peters formula.[22] We implemented the algorithms given by Tripathi[23] and by Sihver,[24] respectively, and verified them against the few experimental data available in the literature. Figure 6 shows the comparison of calculated and measured total reaction cross sections. For proton targets, the Tripathi formula gives considerably better agreement, within the error bars. In addition to ^{16}O, we chose ^{12}C as a representative for heavier targets. For these targets, the difference between the two algorithms is less pronounced at lower energies, but still the Tripathi curves are closer to the experimental data. Thus, we prefer the Tripathi formula for ^{16}O and ^{12}C as well. One should note, however, the relatively large spread of the experimental values, which leaves some room for the modification of cross section formulae. Furthermore, one should note the large gap between 100 and 400 MeV/u, which unfortunately coincides with the range of therapeutical interest, i.e., 50–200 MeV/u, as well as with the "dip" in the calculated cross section curve.

2.C.2. Fragmentation cross sections

Fortunately only a limited number of reaction channels exists for ^{4}He collisions with hydrogen. They are summarized in Table II, together with their threshold energies.

To calculate the cross sections for fragments created in the breakup channels we follow the propositions in Ref. 21 and obtain the phenomenological formulae

$$\sigma_{^3He} = 47.5\left(\frac{2}{1+e^{(T_{th}-T)/9}}-1\right)\left(1-\frac{0.3}{1+8e^{-T/39}}\right)^3 \times \left(1+0.70\sqrt{T/520}\right)e^{-(T-780)/4300}, \quad (1)$$

$$\sigma_{^3H} = 8.83\left(\frac{2}{1+e^{(T_{th}-T)/7.3}}-1\right)\left(1-\frac{0.3}{1+7e^{-T/73}}\right)^3 \times \left(1+6.54\sqrt{T/550}\right)e^{-(T-750)/4383}, \quad (2)$$

$$\sigma_{^2H} = 17\left(\frac{2}{1+e^{(T_{th}-T)/12}}-1\right)\left(1+\frac{0.21(T/145-1)}{1+e^{(145-T)/6}}\right)e^{-T/3000}, \quad (3)$$

where T is the projectile energy (in MeV/u) and T_{th} the respective threshold energy from Table II.

The breakup cross sections are completed by adding the "pickup" contributions for ^{2}H and ^{3}He:

$$\sigma_{Pickup} = 48e^{-(T-T_{th})^{1.7}/1350}. \quad (4)$$

For the remaining cross section for ^{1}H production no model description exists, thus we estimate it from the already known cross sections as[34]

$$\sigma_{^1H} = \frac{3}{5}\left(\sigma_R - \sigma_{Pickup,^3He} + \sigma_{^3H} - 0.5\sigma_{^3He} - 0.5\sigma_{Pickup,^2H} - \frac{1}{3}\sigma_{^2H}\right) \quad (5)$$

by balancing the reaction channels in Table II.

We compare the obtained cross sections with experimental data in Fig. 7. The agreement is acceptable, considering the data sparsity and their relatively large uncertainties.

For heavier targets, a scaling procedure was adopted using empirical factors roughly proportional to the target nucleus radius, i.e., $\propto A^{1/3}$.[21,35] The scaling factors are collected in Table III.

Experimental fragmentation cross sections for oxygen targets were not available, so we verified against experimental data from ^{12}C targets (Fig. 8). The agreement is acceptable considering the few data points and their error bars.

2.D. Biological effect calculation

Our TPS calculates radiobiological effects by separating variable quantities like field directions and particle fluence maps from invariant base data such as the linear–quadratic

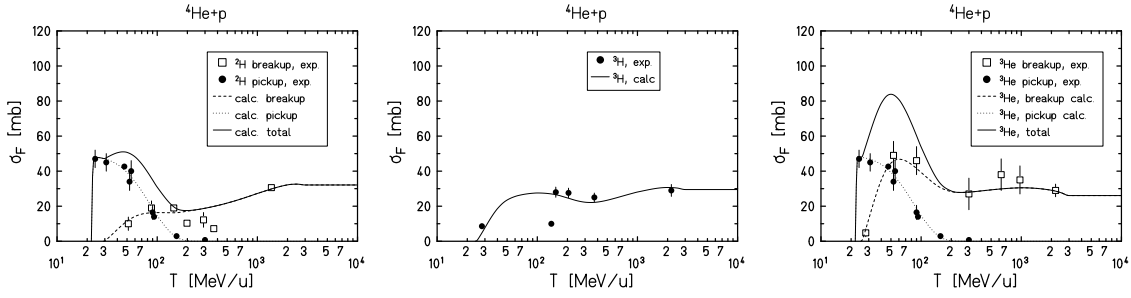

FIG. 7. Fragmentation cross sections for ^{2}H, ^{3}H, and ^{3}He in ^{4}He-p collisions. Symbols are experimental data taken from Ref. 33.

TABLE III. Scaling factors for σ_F in ^{4}He–carbon (oxygen) collisions.

Cross section	Scaling factor
$\sigma_{^1\mathrm{H}}$	$A_T^{0.46}$
$\sigma_{^2\mathrm{H}}$	$A_T^{0.4}$, $A_T^{1/3}$ (pickup)
$\sigma_{^3\mathrm{H}}$	$A_T^{0.31}$
$\sigma_{^3\mathrm{He}}$	$A_T^{0.31}$, $A_T^{1/3}$ (pickup)

(LQ) model parameters for single particle traversal, α_z, β_z. The algorithms how to combine these in order to obtain macroscopic quantities such as cell survival, lethal effect, and the associated RBE are described elsewhere.[37] The single particle α_z, β_z tables are externally supplied by means of the Local Effect Model (LEM) in version IV.[16] This version is based on a fine tuned partitioning between isolated and clustered DNA double strand breaks caused by the local dose deposition. As a consequence, it describes more adequately the different effectiveness of low- and high-LET radiations, respectively. So, unlike its predecessors, LEM IV is particularly suited to describe radiobiological effects of lower LET radiation such as protons and helium ions.

3. RESULTS

3.A. Transport calculation

Using the cross sections calculated as described in the previous section, we can perform transport calculations as described elsewhere.[6,7] In a first test, we compare with measurements of the primary beam attenuation and the build up of projectile fragments as the beam traverses thicker slabs of water (Fig. 9). These observables can simply be obtained numerically using the nuclear interaction cross sections and the electromagnetic energy loss discussed earlier, there is no need to involve intransparent Monte Carlo codes. Within the experimental uncertainties, we find good agreement for the primary beam and ^{3}He. In particular the agreement of the primary beam attenuation up to 8 cm, corresponding to beam energies between 200 and 160 MeV/u, confirms the total reaction cross sections assumed in Fig. 6. Hydrogen isotopes, in particular protons, however, are overestimated by the calculation by a factor of roughly two. These discrepancies remain, although experimental uncertainties such as limited angular acceptance, energy thresholds in the detectors and self pile-up of protons are accounted for. This is not too surprising, since the hydrogen isotope production especially for oxygen targets is only estimated by means of the semiempirical factors in Table III. These factors are only weakly confirmed for carbon targets, Fig. 8, and we have no independent confirmation for oxygen targets. Of course one could start to modify Table III for oxygen targets to obtain better agreement with the measurements, but we decided not to do so. On the other hand, the hydrogen isotopes do not contribute much to the absorbed dose or cell survival. In order to estimate the influence of suboptimal hydrogen cross sections, we performed a sensitivity analysis of the resulting cell survival calculations, presented in Subsection 3.C.

Depth dose profiles (planar integrated dose distributions) serve as a further cross check for the model validity. Unfortunately, at the time of the model development only legacy data from the LBNL radiotherapy project were available for comparison. Experimental details were not available, so some plausible assumptions had to be made. Figure 10 shows our model calculations for two energies of therapeutical interest in comparison with experimental data.[38] The experimental data were shifted by 9.6 mm to match the predicted position of the Bragg peak(s). We consider this to be justified since the properties of the beam delivery (e.g., boli in the beam path) are not known and calculations of the Bragg peak position are believed to be reliable. Unfortunately only few data points beyond the peak are available (at 150 MeV/u) to verify the fragmentation tail contribution, but the agreement is acceptable.

3.B. Absorbed dose verification

The physical beam model is verified by a set of absorbed dose measurements in depth as well as in lateral direction. For extended target volumes the absorbed dose distribution is calculated using established pencil beam algorithms[6] which include multiple Coulomb scattering, the angular distribution

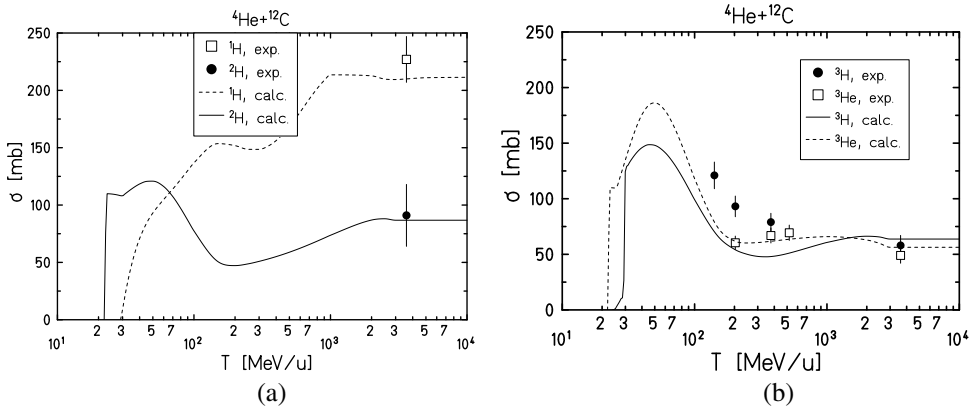

FIG. 8. Fragmentation cross sections for ^{1}H, ^{2}H and ^{3}H, ^{3}He in ^{4}He-^{12}C collisions. Symbols are experimental data taken from Ref. 35 (a) and Refs. 35 and 36 (b).

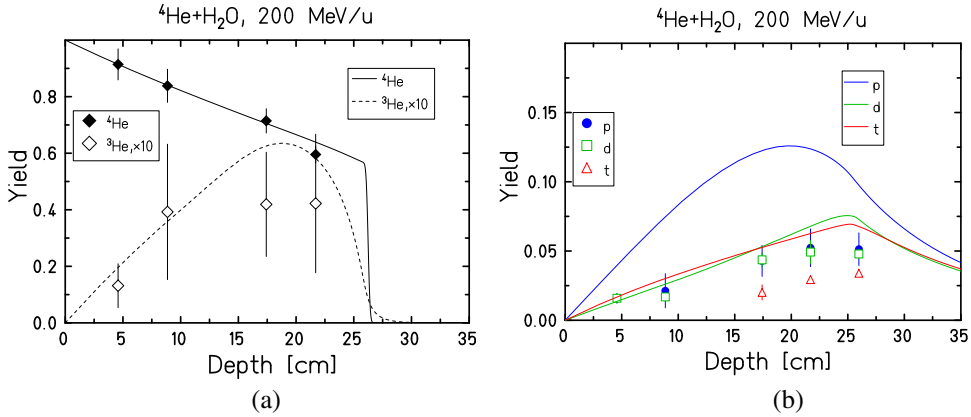

FIG. 9. Attenuation and fragment build up of a ^{4}He beam of 200 MeV/u as a function of depth in water. Symbols represent measurements with the setup described in Subsection 2.B.2, while the curves are our transport calculations.

of nuclear fragments, and the divergence of the beam at depths far off the assumed isocenter. Figure 11 reports results for a 30×50 mm^2 target volume covering a depth of 40 mm. Inset (a) shows depth dose distributions taken along a cut traversing the target volume through the isocenter. The agreement with the prediction (blue curve) is about 3% in the target volume, about 9% at the distal edge, and about 5% in the entrance channel.

In Fig. 11(a) we have added another set of absorbed dose measurements, corresponding directly to the cell survival measurement shown in Fig. 12 (red symbols). The target volume was slightly different, but comparable, whereas the planned dose level in the target was 4 Gy (scaled down to 1 Gy in Fig. 11). The deviation at the distal edge of the target volume is much less than in the previous case. The two sets of measurements differ by ≈2%, which might serve as an indication of the intrinsic uncertainty of the experiment.

Figure 11(b) shows lateral dose distributions taken at 15.8 and 68 mm depth, respectively. The overall agreement is good, with an underestimation of the central dose corresponding to the deviations seen in 11(a). There is a noticeable deviation at the edges of the target volume, which also needs further investigation.

Since this is a first set of measurements, it is still under investigation whether the observed deviations arise from shortcomings of the applied beam model or the experimental conditions, such as beam spot size, beam divergence, or calibration of the scanning system.

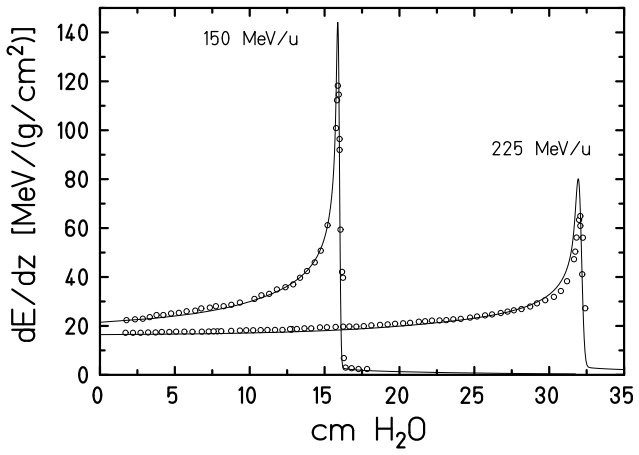

FIG. 10. Depth dose profiles for ^{4}He beams of two energies. Symbols are experimental data reproduced from J. Lyman and J. Howard, "Dosimetry and instrumentation for helium and heavy ions," Int. J. Radiat. Oncol. Biol. Phys. **3**, 81–85 (1977).

3.C. Biological dose verification

Figure 12 presents the results of the biological verification measurements, performed with the experimental setup described in Sec. 2. A 60×100 mm^2 target volume centered at a depth of 82 mm was irradiated with a homogeneous absorbed dose of 4 Gy, i.e., with a plan optimized on uniform absorbed dose all along the target. The corresponding nonhomogeneous survival distribution was forward calculated using two different sets of α_x and β_x to characterize the linear–quadratic X-ray survival curve used as the reference radiation for LEM IV. One set, labeled "mean," represents the average of α_x, β_x values for the used cell line, taken over the last five years (α_x,β_x = 0.171,0.02). The other set, labeled "2014," was specifically obtained during an X-ray calibration measurement a few days before the ^{4}He experiments (α_x,β_x = 0.1,0.034). Within experimental error bars, both calculations give good agreement with the experimental results. The two calculations differ by approximately 8% in survival level, demonstrating the natural time variation of radiosensitivity for the CHO cell line used.

3.C.1. Sensitivity analysis with regard to absorbed dose deviations

It is conceivable that the deviations between measured and predicted absorbed dose, Fig. 12(a), in particular at the distal edge, could affect the validity of the biological predictions. We thus provide an additional depth survival profile based on an absorbed dose distribution adapted to the measured data. The difference to the nominal survival rate is between 5% and 10% in the target region, but still within the error bars of the experimental survival values. Hence one of the main

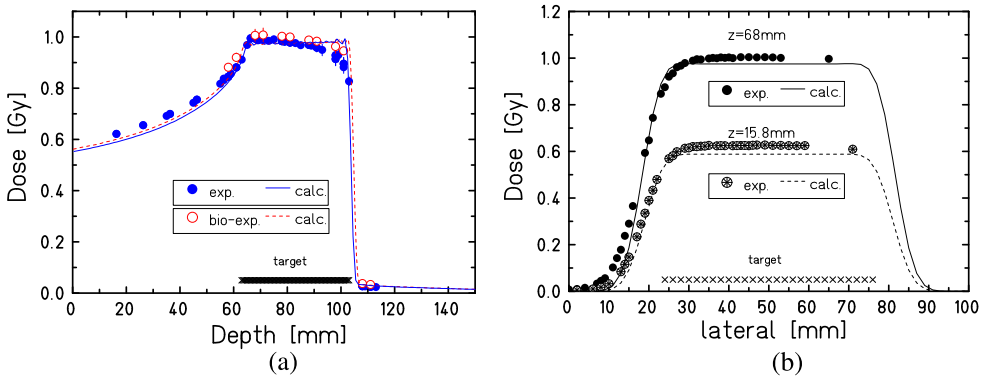

FIG. 11. (a) Depth dose distributions for a target volume at 83 mm depth, covering a depth range of 40 mm (blue symbols) The open symbols correspond to the plan used for the biological measurement shown in Fig. 12, scaled down by a factor 4. The solid curves are the respective TPS predictions. (b) Lateral dose profiles taken at 15.8 and 68 mm depth, respectively. The solid curves are the TPS predictions.

conclusions, i.e., the steep rise of RBE toward the distal edge, remains valid.

3.C.2. Sensitivity analysis with regard to fragment contributions

Since the used nuclear fragmentation cross sections have a rather large uncertainty we performed a sensitivity analysis in order to estimate their influence on the depth survival profile, Fig. 13(b). It turns out that their influence is vanishing in the entrance channel as well as at the distal edge, as it should be, since at these positions the primary beam dominates. The largest effect arises from the ^{3}He contribution in the proximal and central part of the target volume. There, the survival rate may change by 10% (e.g., from 0.32 to 0.35) when ^{3}He is excluded from the calculation. The hydrogen isotopes play only a minor role, on the order of 5% altogether, and the influence of protons [from the red to the blue curve in Fig. 13(b)] is hardly visible.

3.C.3. Comparison with the literature data

We also looked for comparisons with the literature data, in particular from the pioneering research at LBNL. This is not straightforward given the historical time frame, and the vastly different experimental setups. For human T-1 cells irradiated with 70 Gy equivalent to ^{60}Co in five fractions an overall RBE of 1.3 for cell killing is reported for a simulated tumor location (from 1.5 to 2.5 cm depth in water).[39] Another experiment reports RBE values of 1.2 ± 0.2 determined at the center of a target volume extending from 10.5 to 21 cm, irradiated with 5.5 Gy.[40] These RBE values are compatible with our findings, at least in the center of the target volume. One should keep in mind, however, that their experimental conditions are quite different from ours as far as cell lines, dose per fraction, and simulated tumor locations are concerned. Certainly the static RBE values used at LBNL were appropriate at their time. However, RBE values depend on dose level, irradiation geometry, and tissue type. With today's 3D active scanning technique, it is mandatory to assign an individual RBE value to each irradiated voxel. Even if the rise of RBE at the distal edge would be less pronounced, due to the absorbed dose deviations discussed above, the assumption of a constant RBE is no longer appropriate, since the measured depth survival values vary by a factor of four. Moreover, a strong rise of RBE will also influence the effective range at the distal edge of the target volume.[41]

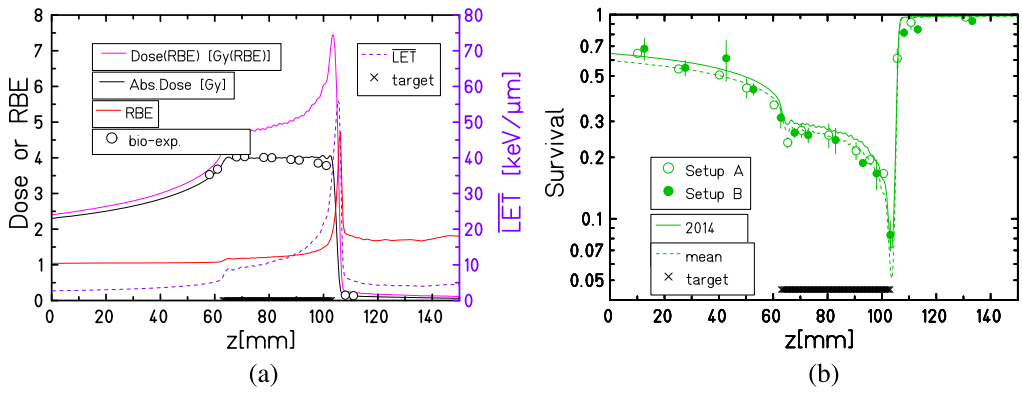

FIG. 12. Depth profiles for the biological verification, with the target volume centered at 82 mm depth, covering a depth range of 40 mm. (a) Calculated absorbed dose, RBE-weighted dose, RBE and dose-averaged LET depth profile. The symbols represent absorbed dose measurements performed with the setup described in Subsection 2.B.3 in a different run but with the same treatment plan. (b) Depth survival profile, symbols represent measurements with different setups, the two curves are predictions by our TPS using different values of α and β of the reference radiation.

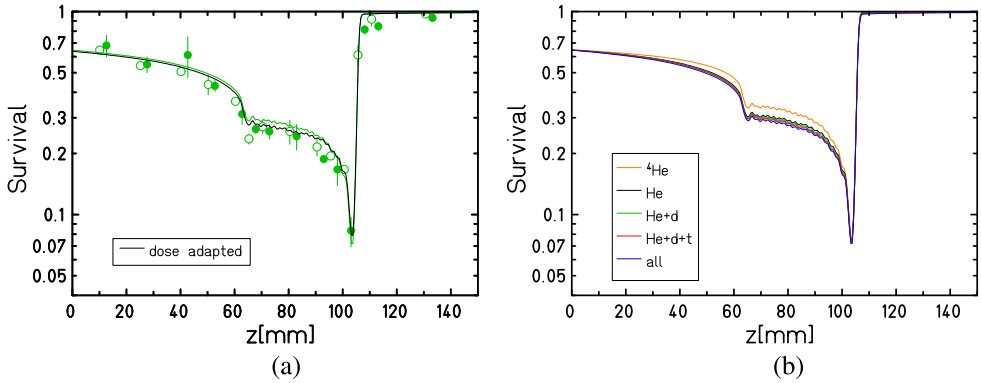

FIG. 13. Sensitivity analysis of the survival profile for the "2014" case in Fig. 12(b). (a) With a dose profile adapted to the measured absorbed dose in Fig. 12(a). (b) With respect to nuclear fragment contributions.

4. DISCUSSION AND CONCLUSIONS

The agreement between biological verification data and TPS prediction shows that a pragmatic physical beam model together with the radiobiological model can be used to provide realistic ^{4}He ion treatment plans. In particular, the well reproduced strong variation of cell survival around 105 mm depth, which usually is hard to catch, gives good confidence in the overall accuracy of the chosen modeling.

Realistic treatment plans are mandatory for future comparisons between different ion beam modalities. Although advantages and disadvantages might be estimated from simple physical and radiobiological properties of the single ions, full treatment plans under patient conditions often enough reduce or modify the theoretical differences between the various ion modalities. As it has been shown by Grün *et al.*,[42] who used our TPS to compare protons, ^{4}He and ^{12}C ions, respectively, there is no unique choice for an optimal ion species. It largely depends on patient specific parameters such as field configuration, α and β values and even the prescribed dose level.

Extensive comparative planning studies, however, are beyond the scope of this contribution and are left for future research.

Other directions for future experimental investigation are the necessity to clarify the deviations between absorbed dose measurements and TPS predictions, as well as filling the cross section data gap in the therapeutic region between 50 and 200 MeV/u.

Last but not least more patient-like biological verification measurements are planned, covering survival distributions in two dimensions as well as lateral survival distributions.

ACKNOWLEDGMENTS

The authors like to thank Frederike Schmitz, whose Master Thesis contributed significantly to the physical beam model described in this paper. The authors like to thank Daniel Richter and Ralf Panse for their assistance during the HIT runs, as well as the HIT accelerator crew for excellent technical assistance during beamtime and the HIT program advisory committee for their generous support to the experiment.

[a]Author to whom correspondence should be addressed. Electronic mail: m.kraemer@gsi.de

[1]W. Saunders *et al.*, "Helium-ion radiation therapy at the Lawrence Berkeley Laboratory: Recent results of a Northern California Oncology Group clinical trial," Radiat. Res. **104**, S227–S234 (1985).
[2]S. Combs, O. Jäkel, T. Haberer, and J. Debus, "Particle therapy at the Heidelberg Ion Therapy Center (HIT)–Integrated research-driven university-hospital-based radiation oncology service in Heidelberg, Germany," Radiother. Oncol. **95**, 41–44 (2010).
[3]S. Rossi, "The status of CNAO," Eur. Phys. J. Plus **126**, 1–39 (2011).
[4]M. Benedikt and A. Wrulich, "Medaustron–project overview and status," Eur. Phys. J. Plus **126**, 1–11 (2011).
[5]M. Jermann, "Particle therapy statistics in 2014," Int. J. Part. Ther. **2**, 50–54 (2015).
[6]M. Krämer and M. Durante, "Ion beam transport calculations and treatment plans in particle therapy," Eur. Phys. J. D **60**, 195–202 (2010).
[7]M. Krämer, O. Jäkel, T. Haberer, G. Kraft, D. Schardt, and U. Weber, "Treatment planning for heavy-ion radiotherapy: Physical beam model and dose optimization," Phys. Med. Biol. **45**, 3299–3317 (2000).
[8]M. Krämer and M. Scholz, "Treatment planning for heavy-ion radiotherapy: Calculation and optimization of biologically effective dose," Phys. Med. Biol. **45**, 3319–3330 (2000).
[9]D. Schardt, T. Elsässer, and D. Schulz-Ertner, "Heavy-ion tumor therapy: Physical and radiobiological benefits," Rev. Mod. Phys. **82**, 383 (2010).
[10]E. Scifoni, W. Tinganelli, W. K. Weyrather, M. Durante, A. Maier, and M. Krämer, "Including oxygen enhancement ratio in ion beam treatment planning: Model implementation and experimental verification," Phys. Med. Biol. **58**, 3871–3895 (2013).
[11]M. Krämer, E. Scifoni, F. Schmitz, O. Sokol, and M. Durante, "Overview of recent advances in treatment planning for ion beam radiotherapy," Eur. Phys. J. D **68**, 1–6 (2014).
[12]E. Haettner, H. Iwase, M. Krämer, G. Kraft, and D. Schardt, "Experimental study of nuclear fragmentation of 200 and 400 MeV/u 12C ions in water for applications in particle therapy," Phys. Med. Biol. **58**, 8265–8279 (2013).
[13]K. Gunzert-Marx, H. Iwase, D. Schardt, and R. Simon, "Secondary beam fragments produced by 200 MeV/u 12C ions in water and their dose contributions in carbon ion radiotherapy," New J. Phys. **10**, 075003 (2008).
[14]C. P. Karger, O. Jäkel, G. H. Hartmann, and P. Heeg, "A system for three-dimensional dosimetric verification of treatment plans in intensity-modulated radiotherapy with heavy ions," Med. Phys. **26**, 2125–2132 (1999).
[15]C. P. Karger, O. Jäkel, H. Palmans, and T. Kanai, "Dosimetry for ion beam radiotherapy," Phys. Med. Biol. **55**, R193–R234 (2010).
[16]T. Elsässer *et al.*, "Quantification of the relative biological effectiveness for ion beam radiotherapy: Direct experimental comparison of proton and carbon ion beams and a novel approach for treatment planning," Int. J. Radiat. Oncol., Biol., Phys. **78**, 1177–1183 (2010).
[17]W. Weyrather, S. Ritter, M. Scholz, and G. Kraft, "RBE for carbon track-segment irradiation in cell lines of differing repair capacity," Int. J. Radiat. Biol. **75**, 1357–1364 (1999).
[18]H. Fuchs, J. Ströbele, T. Schreiner, A. Hirtl, and D. Georg, "A pencil beam algorithm for helium ion beam therapy," Med. Phys. **39**, 6726–6737 (2012).

[19]M. Salamon, "Range-energy program for relativistic heavy ions in the region 1 < E < 3000 MeV/amu," Lawrence Berkeley National Laboratory Paper No. 10446, 1980.
[20]R. Silberberg and C. Tsao, "Spallation processes and nuclear interaction products of cosmic rays," Phys. Rep. **191**, 351–408 (1990).
[21]F. A. Cucinotta, L. W. Townsend, and J. W. Wilson, "Description of alpha-nucleus interaction cross sections for cosmic ray shielding studies," NASA Technical Paper No. 3285, 1993.
[22]H. Bradt and B. Peters, "The heavy nuclei of the primary cosmic radiation," Phys. Rev. **77**, 54–70 (1950).
[23]R. Tripathi, F. Cucinotta, and J. Wilson, "Accurate universal parameterization of absorption cross sections III–light systems," Nucl. Instrum. Methods Phys. Res., Sect. B **155**, 349–356 (1999).
[24]L. Sihver and D. Mancusi, "Present status and validation of HIBRAC," Radiat. Meas. **44**, 38–46 (2009).
[25]R. F. Carlson, "Proton–nucleus total reaction cross sections and total cross sections up to 1 GeV," At. Data Nucl. Data Tables **63**, 93–116 (1996).
[26]A. M. Sourkes, "Total reaction cross section for protons on ^{3}He and ^{4}He between 18 and 48 MeV," Phys. Rev. C **13**, 451 (1976).
[27]W. R. Webber, "Individual isotopic fragmentation cross sections of relativistic nuclei in hydrogen, helium, and carbon targets," Phys. Rev. C **41**, 520 (1990).
[28]J. Jaros *et al.*, "Nucleus–nucleus total cross sections for light nuclei at 1.55 and 2.89 Gev/c per nucleon," Phys. Rev. C **18**, 2273–2292 (1978).
[29]P. Ferrando, W. Webber, P. Goret, J. Kish, D. Schrier, A. Soutoul, and O. Testard, "Measurement of ^{12}C, ^{16}O, and ^{56}Fe charge changing cross sections in helium at high energy, comparison with cross sections in hydrogen, and application to cosmic-ray propagation," Phys. Rev. C **37**, 1490–1501 (1988).
[30]A. Auce *et al.*, "Reaction cross sections for 75–190 MeV alpha particles on targets from ^{12}C to ^{208}Pb," Phys. Rev. C **50**, 871–879 (1994).
[31]A. Ingemarsson *et al.*, "New results for reaction cross sections of intermediate energy α-particles on targets from ^{9}Be to ^{208}Pb," Nucl. Phys. A **676**, 3–31 (2000).
[32]S. Fiarman and W. Meyerhof, "Energy levels of light nuclei A=4," Nucl. Phys. A **206**, 1–64 (1973).
[33]J. Meyer, "Deuterons and ^{3}He formation and destruction in proton induced spallation of light nuclei (Z<= 8)," Astron. Astrophys. Suppl. Ser. **7**, 417–467 (1972).
[34]F. Schmitz, "A semiempirical beam model for ^{4}He projectiles in ion beam radiotherapy," Master thesis, University Heidelberg, 2013.
[35]A. Abdurakhimov and M. Anikina, "A study of pion production in 4.5 (GeV/c)/nucleon ^{4}He interactions with nuclear targets," Nucl. Phys. A **362**, 376–390 (1981).
[36]W. R. Webber, "New measurements of the cross sections of He-4 into H-2 and He-3 and their implication for H-2 and He-3 production in cosmic rays," in *Particle Astrophysics - The NASA Cosmic Ray Program for the 1990s and Beyond* (American Institute of Physics, New York, 1990), pp. 294–298.
[37]M. Krämer and M. Scholz, "Rapid calculation of biological effects in ion radiotherapy," Phys. Med. Biol. **51**, 1959–1970 (2006).
[38]J. Lyman and J. Howard, "Dosimetry and instrumentation for helium and heavy ions," Int. J. Radiat. Oncol., Biol., Phys. **3**, 81–85 (1977).
[39]W. Saunders, D. Char, J. Quivey, J. Castro, G. Chen, J. Collier, A. Cartigny, E. Blakely, J. Lyman, S. Zink, and T. Tobias, "Precision, high dose radiotherapy: Helium ion treatment of uveal melanoma," Int. J. Radiat. Oncol., Biol., Phys. **11**, 227–233 (1985).
[40]M. Raju, E. Bain, S. Carpenter, R. A. Cox, and J. Robertson, "A heavy particle comparative study. Part II: Cell survival versus depth," Br. J. Radiol. **51**, 704–711 (1978).
[41]R. Grün, T. Friedrich, M. Krämer, K. Zink, M. Durante, R. Engenhart-Cabillic, and M. Scholz, "Physical and biological factors determining the effective proton range," Med. Phys. **40**, 1716 (2013).
[42]R. Grün, T. Friedrich, M. Krämer, K. Zink, M. Durante, R. Engenhart-Cabillic, and M. Scholz, "Assessment of potential advantages of relevant ions for particle therapy: A model based study," Med. Phys. **42**, 1037 (2015).